

Quantum phase space theory for the calculation of $\mathbf{v} \cdot \mathbf{j}$ vector correlations

Simon W. North and Gregory E. Hall

Department of Chemistry, Brookhaven National Laboratory, Upton, New York 11973-5000

(Received 25 September 1995; accepted 23 October 1995)

The quantum state-counting phase space theory commonly used to describe “barrierless” dissociation is recast in a helicity basis to calculate photofragment $\mathbf{v} \cdot \mathbf{j}$ correlations. Counting pairs of fragment states with specific angular momentum projection numbers on the relative velocity provides a simple connection between angular momentum conservation and the $\mathbf{v} \cdot \mathbf{j}$ correlation, which is not so evident in the conventional basis for phase space state counts. The upper bound on the orbital angular momentum, l , imposed by the centrifugal barrier cannot be included simply in the helicity basis, where l is not a good quantum number. Two approaches for an exact calculation of the $\mathbf{v} \cdot \mathbf{j}$ correlation including the centrifugal barrier are described to address this point, although the simpler helicity state count with no centrifugal barrier correction is remarkably good in many cases. An application to the photodissociation of NCCN is consistent with recent classical phase space calculations of Klippenstein and Cline. The experimentally observed vector correlation exceeds the phase space theory prediction. We take this as evidence of incomplete mixing of the K states of the linear parent molecule at the transition state, corresponding to an evolution of the body-fixed projection number K into the total helicity of the fragment pair state. The average over a thermal distribution of parent angular momentum in the special case of a linear molecule does not significantly reduce the $\mathbf{v} \cdot \mathbf{j}$ correlation below that computed for total $J=0$. Predictions of the $\mathbf{v} \cdot \mathbf{j}$ correlations for the unimolecular dissociation of NCNO and CH_2CO are also provided. © 1996 American Institute of Physics. [S0021-9606(96)00305-X]

I. INTRODUCTION

Phase space theory¹ offers a simple and intuitive reference point for viewing possible dynamic effects in unimolecular and bimolecular reactions. For reactions with no barriers, the transition state resembles separated product states, and a detailed transition state rate calculation can often be replaced by an appropriate state count of the products, consistent with energy and angular momentum conservation. Phase space theory has been compared with varying degrees of success to measured rotational and vibrational state distributions, translational energy distributions, threshold photofragment excitation spectra, and absolute reaction rates.²⁻⁴ The connection between phase space theory and vector correlations is less well known. Recently, moderately strong $\mathbf{v} \cdot \mathbf{j}$ correlations were measured in the predissociation of NCCN,⁵ historically considered a prototypical statistical reaction. We have sought a means of calculating the statistically expected $\mathbf{v} \cdot \mathbf{j}$ correlations in order to assess dynamic effects in this and other photodissociations. Klippenstein and Cline⁶ have recently used Monte Carlo methods to generate representative classical phase space ensembles from which vector correlations have been extracted. They present useful generalizations about the statistical expectations for photofragment $\mathbf{v} \cdot \mathbf{j}$ correlations, based on the relative moments of inertia of two reaction products and on the total angular momentum. Classical phase space theory has the advantage of wide applicability, as the computational effort does not grow as quickly with energy and molecular complexity as does a direct state count.

In the present paper, we describe a quantum phase space theory, using a traditional state-counting technique, but making explicit the statistical expectations for the $\mathbf{v} \cdot \mathbf{j}$ correlation. A preliminary version of this work has been published.⁷ In the bipolar moment language applied by Dixon⁸ to the Doppler spectroscopy of photofragments, the leading term in the $\mathbf{v} \cdot \mathbf{j}$ correlation is $\beta_0^0(22)$, which is the ensemble average of $P_2(\hat{\mathbf{v}} \cdot \hat{\mathbf{j}})$, where $P_2(x) = \frac{1}{2}(3x^2 - 1)$ and $\hat{\mathbf{v}}$ is the unit vector along the recoil velocity of a fragment with a rotational angular momentum in the direction $\hat{\mathbf{j}}$. Calculation of $\langle P_2(\hat{\mathbf{v}} \cdot \hat{\mathbf{j}}) \rangle$ lends itself to working in a basis for which the projection of \mathbf{j} on the relative velocity is a good quantum number. A helicity basis set, first described by Jacob and Wick⁹ in the context of nuclear scattering theory for particles with intrinsic spin, has this property, and provides an intuitive simplicity to state counting when Legendre moments of the helicity are the desired observables.

The outline of the paper is as follows. Section II A briefly describes the conventional phase space theory developed by Pechukas and Light, and a procedure for calculating $\mathbf{v} \cdot \mathbf{j}$ correlations in the traditional basis. In Sec. II B the direct state count in the helicity basis is introduced as an approximate, but very efficient and intuitive method to predict $\mathbf{v} \cdot \mathbf{j}$ correlations. A correction required to obtain the exact phase space theory from the approximate helicity state count is described in Sec. II C. A set of simple pedagogical examples for low state counts is presented in Sec. III. The theory is then applied to three benchmarks of statistical unimolecular dissociation: NCCN, NCNO, and CH_2CO .

II. THEORY

A. Transformed phase space theory

The statistical phase space theory is applied to the breakup of a molecular complex with a specific energy E , and total angular momentum J . The probability of producing fragment i in electronic and vibrational state v_i and rotational state j_i is given by the number of such states, $N(v_i, j_i, E, J)$, normalized by the total number of accessible states $N(E, J)$

$$P_{v_i, j_i}(E, J) = \frac{N(v_i, j_i; E, J)}{N(E, J)}. \quad (1)$$

Klippenstein⁶ has provided a compact notation for the evaluation of the state counts for two diatomic fragments

$$N(E, J) = \sum_{v_1, j_1, v_2, j_2, l, j, M} \Theta[E - E_1(v_1, j_1) - E_2(v_2, j_2) - E_{12}^\dagger(l)] \times \Delta(J, j, l) \Delta(j, j_1, j_2), \quad (2)$$

where j_i is the angular momentum for fragment i , l is the orbital angular momentum, j is the net angular momentum of $j_1 + j_2$, and M is a space-fixed projection of total angular momentum, J . The Heaviside function, Θ , ensures counting only states that conserve energy, including the l -dependent rotational kinetic energy at the centrifugal barrier, E_{12}^\dagger . Angular momentum conservation is represented by a set of triangle inequalities,

$$\Delta(i, j, k) = \begin{cases} 1 & \text{if } |i - j| \leq k \leq (i + j) \\ 0 & \text{otherwise} \end{cases}, \quad (3)$$

restricting the values of j and l for given j_1, j_2 , and J . The energy at the top of the centrifugal barrier is usually written as

$$E_{12}^\dagger(l) = 2 \left[\frac{l(l+1)\hbar^2}{6\mu C_6^{1/3}} \right]^{3/2}, \quad (4)$$

where C_6 is the coefficient of the spherically averaged, r^{-6} dependent, attractive interaction potential and μ is the reduced mass of the two fragments. This is appropriate at low kinetic energies, when the centrifugal barrier is at large enough fragment separation to ignore the contributions of chemical bonding and repulsion to the total interaction potential. For more general forms of the attractive potential than a simple r^{-6} dependence, $E_{12}^\dagger(l)$ can instead be expressed as

$$E_{12}^\dagger(l) = \frac{l(l+1)\hbar^2}{2\mu b_{\max}^2}, \quad (5)$$

where b_{\max} is the maximum impact parameter allowed by the centrifugal barrier. Although b_{\max} is strictly a weak function of the kinetic energy, it is common practice to describe the effect of the centrifugal barrier with a fixed value of b_{\max} .

In the original formulation¹ for breakup of a triatomic complex, $ABC \rightarrow A + BC$, the only angular momenta involved are l for the orbital angular momentum, j for the diatomic rotation, and J for the total angular momentum. The

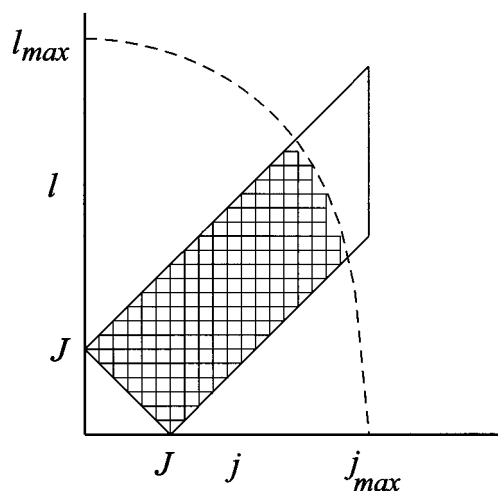


FIG. 1. Conventional state count for $A + BC$ at fixed total J comes from the number of interior jl lattice points. The dashed line represents the energy conservation boundary imposed by the centrifugal barrier.

state counts in this case are graphically depicted as the number of lattice points in the jl plane. Figure 1 shows a typical jl plane for fixed value of J . Three diagonal linear boundaries arise from angular momentum conservation, while the vertical line at j_{\max} represents the total available energy going into the rotation of BC . The dashed, curved boundary arises from energy conservation including the upper bound on l due to the centrifugal barrier.

The generalization to fragmentation of a four-atom complex into a pair of diatomic fragments, $ABCD \rightarrow AB + CD$, has been treated by Dagdigian *et al.*¹⁰ and by Wittig *et al.*¹¹ The state counts are only slightly more complex, as indicated in Eq. (2). Now the counting can be graphically represented as lattice points in a jl plane, where j is the resultant of $\mathbf{j}_1 + \mathbf{j}_2$, and the plot is for fixed values of J, j_1 , and j_2 . Figure 2 shows the jl plane for $J=3, j_1=3$, and $j_2=4$. The upper and lower bounds on j are indicated as vertical dashed lines.

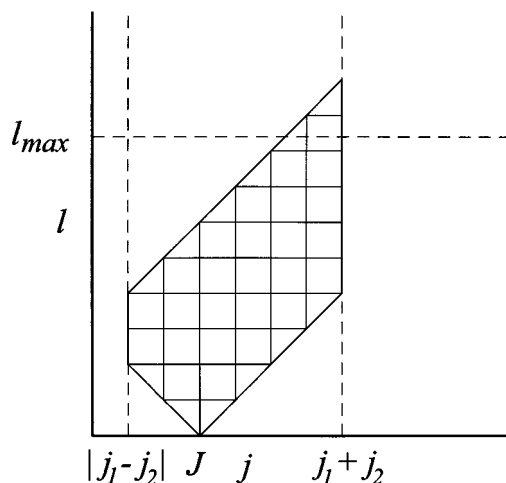


FIG. 2. Conventional state count for a pair of diatomic fragments for fixed total J, j_1 , and j_2 . The region of summation is shown for values $J=3, j_1=3$, and $j_2=4$.

Since the kinetic energy is equivalent for all the states counted in this figure, the upper bound on l is a horizontal line, independent of j . The upper bound on l derived from the centrifugal barrier may or may not be more restrictive than the angular momentum restrictions alone.

Although a state count in the traditional jl basis is appropriate for predicting product state distributions, calculation of the vector correlation of fragment velocity and rotational angular momentum is awkward. A helicity basis, as described by Jacob and Wick⁹ lends itself to a direct quantum evaluation of the $\mathbf{v} \cdot \mathbf{j}$ correlation, since the projections of fragment angular momenta on the recoil axis are good quantum numbers in this basis. The l and j quantum numbers are transformed to helicity quantum numbers, λ_i , denoting the projections of angular momentum on the center-of-mass relative velocity. Along this unique axis, the orbital angular momentum necessarily has zero projection. A complete set of quantum numbers specifying the same breakup to two fragment states includes total J and its space-fixed projection number M , the magnitudes of two fragment angular momenta, j_1 and j_2 , and the two fragment helicities, λ_1 and λ_2 . The total helicity, $\Lambda = \lambda_1 - \lambda_2$ is independent of the orbital angular momentum. Transforming a state count in the jl basis into the helicity representation to extract $\mathbf{v} \cdot \mathbf{j}$ correlations is now considered.

The conventional jl states can be expanded in the helicity basis for each fixed j_1 and j_2 . The elements of the transformation matrix are given by Jacob and Wick⁹

$$\begin{aligned} \langle JM; j_1 l | JM; \lambda_1 \lambda_2 \rangle &= (2l+1)^{1/2} (2j+1)^{1/2} \\ &\times \begin{pmatrix} j_1 & j_2 & j \\ \lambda_1 & -\lambda_2 & -\Lambda \end{pmatrix} \\ &\times \begin{pmatrix} j & l & J \\ \Lambda & 0 & -\Lambda \end{pmatrix}. \end{aligned} \quad (6)$$

The first 3- j symbol treats the coupling of j_1 and j_2 in specific helicity states to give a net angular momentum j and total helicity $\Lambda = \lambda_1 - \lambda_2$. The second treats the coupling of j and l to give J . Note that in the helicity frame only the $m_l = 0$ component of the orbital angular momentum need be considered. The transformation is unitary, and gives immediately, if inefficiently, a method to calculate the quantum phase space prediction for the $\mathbf{v} \cdot \mathbf{j}$ correlation for a fragment in state j_1 . The prescription is as follows: count the states in the jl basis according to Eq. (2), and transform each jl state into its mixed helicity components according to Eq. (6). Accumulate the probability distribution of λ_1 in a histogram, $p(\lambda_1)$, for each jl state included in the conventional phase space state count. When all jl states have been included in the sum, the desired $\mathbf{v} \cdot \mathbf{j}$ correlation is simply the second Legendre moment of the normalized $p(\lambda_1)$ distribution

$$\langle P_2(\hat{\mathbf{v}} \cdot \hat{\mathbf{j}}_1) \rangle = \sum_{\lambda_1 = -j_1}^{j_1} p(\lambda_1) \times P_2 \left(\frac{\lambda_1}{\sqrt{j_1(j_1+1)}} \right). \quad (7)$$

While this method for evaluating $\mathbf{v} \cdot \mathbf{j}$ correlations exactly within traditional phase space theory is straightforward, it

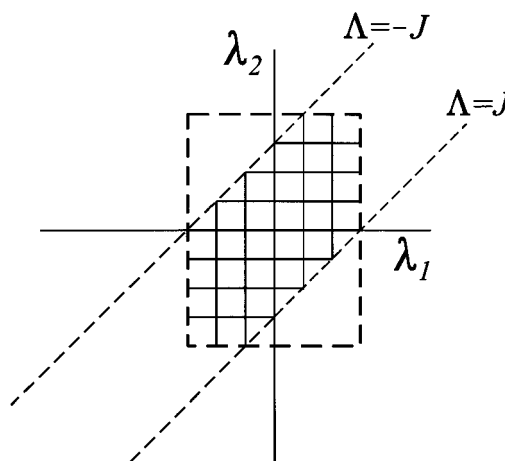


FIG. 3. Helicity state count for the same J , j_1 , and j_2 values as in Fig. 2. The diagonal dashed lines indicate the bounds on the total helicity, $|\Lambda| \leq J$.

requires the calculation of multiple 3- j symbols for each jl state in the count of $N(E, J)$. Even for a tetratomic system with typical j values less than 40, and only one vibrational channel open, the calculation of a $\mathbf{v} \cdot \mathbf{j}$ correlation for a single detected rotational state can easily require the evaluation of more than 10^7 3- j symbols. The 3- j symbols in Eq. (6) can be evaluated using either quantum mechanical recursion relations or a semi-classical approximation.¹² For large values of the arguments the semiclassical treatment provides quantitatively accurate results¹³ for considerably less effort.

B. Helicity state count

If we neglect, for the moment, the upper bound on l due to the centrifugal barrier, we can define $N'(E, J) \geq N(E, J)$ as an upper bound on the true phase space state count, obtained by dropping the centrifugal energy term, E_{12}^\ddagger

$$\begin{aligned} N'(E, J) &= \sum_{v_1, j_1, v_2, j_2, l, j, M} \Theta[E - E_1(v_1, j_1) - E_2(v_2, j_2)] \\ &\times \Delta(J, j, l) \Delta(j, j_1, j_2). \end{aligned} \quad (8)$$

This same sum can be evaluated in the helicity basis

$$\begin{aligned} N'(E, J) &= \sum_{v_1, j_1, \lambda_1, v_2, j_2, \lambda_2, M} \Theta[E - E_1(v_1, j_1) - E_2(v_2, j_2)] \\ &\times \Theta(J - |\lambda_1 - \lambda_2|). \end{aligned} \quad (9)$$

The triangle inequalities involving l and j have been replaced by upper and lower bounds on the total helicity, represented as the Heaviside function of $J - |\Lambda|$. It is to be understood that the summations over projection numbers λ_i are bounded by $\pm j_i$. The helicity state count can be represented graphically for each J, j_1, j_2 as a vertex count in the $\lambda_1 \lambda_2$ plane. Figure 3 shows the $\lambda_1 \lambda_2$ plane for the identical combination of J, j_1 , and j_2 states as in Fig. 2. The independent bounds on fragment helicities define a rectangle with $(2j_1 + 1) \times (2j_2 + 1)$ states. The bounds on $\lambda_1 - \lambda_2$ are represented as diagonals which cross the $\lambda_1 = 0$ axis at $\pm J$. It can be verified that in absence of a centrifugal barrier the corre-

sponding state count in this helicity basis, Eq. (9), is identical to the state count in the conventional jl basis, Eq. (8). Several simple and illustrative examples are shown in Sec. III.

An approximate calculation to obtain $\mathbf{v}\cdot\mathbf{j}$ correlations can be performed directly in the helicity basis with exceeding ease. The calculation provides a qualitatively useful first approximation to the $\mathbf{v}\cdot\mathbf{j}$ correlation and can be corrected with little effort to match the full phase space theory exactly. The helicity state count approach begins by computing $p'(\lambda_1)$ directly from the count of $\lambda_1\lambda_2$ states for a given selected state of fragment 1, v_1 , and j_1 , normalized by the appropriate total count for that state, $N'(v_1, j_1; E, J)$

$$p'(\lambda_1; E, J, v_1, j_1) = \frac{(2J+1)}{N'(v_1, j_1; E, J)} \sum_{v_2, j_2, \lambda_2} \Theta[E - E_1(v_1, j_1) - E_2(v_2, j_2)] \times \Theta(J - |\lambda_1 - \lambda_2|). \quad (10)$$

This calculation involves only integer counting, and is simply a sum over graphs like the one shown in Fig. 3. It can be seen from inspection that only negative $\mathbf{v}\cdot\mathbf{j}$ correlations can arise in this way since the constraints on λ are only in the form of an upper bound on the absolute magnitude. The calculated $\mathbf{v}\cdot\mathbf{j}$ correlation follows directly, using Eq. (7), but with the facile $p'(\lambda)$ approximating the laborious $p(\lambda)$.

C. Correcting the helicity state count for the centrifugal barrier

The correction of the helicity state count to agree exactly with phase space theory requires finding those jl states allowed by angular momentum conservation but rejected by energy conservation at the centrifugal barrier, transforming only those to the helicity basis and removing their contribution from $p'(\lambda_1)$ to compute $p(\lambda_1)$. The states in question are analogous to those shown in Fig. 1 within the trapezoid defined by angular momentum conservation, but at higher l and j than the curved boundary. In Fig. 2, they would be the three states above the dashed line at l_{\max} . Particularly for low J , the number of such states excluded by the centrifugal barrier ($N' - N$) is generally only a small fraction of the number not excluded (N).

We now examine in more detail the effect of the centrifugal barrier at various stages of averaging. The illustrations are prepared for the specific case of NCCN with an assumed available energy of 4700 cm^{-1} . The magnitude of the centrifugal barrier for given j_1 , j_2 , and J was calculated using Eq. (5) with $b_{\max} = 4.0 \text{ \AA}$, in accordance with the estimate of Klippenstein and Cline.⁶ The effects of an unrealistically large centrifugal barrier are also shown, using $b_{\max} = 1.0 \text{ \AA}$. Starting at the most detailed level, Fig. 4 shows an unnormalized helicity distribution, $p(\lambda_1)$, for a detected state $j_1 = 35$ and three single, coincident j_2 states, with the total J fixed at 10. In this figure and the next three, the solid line is the result of the helicity state count (HSC), with no correction applied for the centrifugal barrier. The dashed line includes the correction for our best estimate of the centrifu-

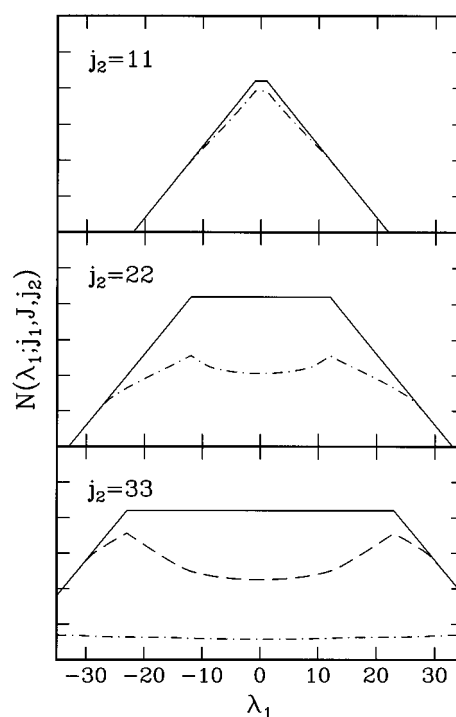


FIG. 4. The number of λ_1 states, $N(\lambda_1)$, for a given coincident j_2 state from a measured $j_1 = 35$ fragment, at total $J = 10$. The solid line is obtained ignoring the centrifugal barrier, the dashed line is obtained with a reasonable placement of the centrifugal barrier at 4.0 \AA , and the dot-dashed line is obtained assuming an unreasonable placement of the centrifugal barrier at 1.0 \AA .

gal barrier (the corrected helicity state count or CHSC). The dot-dashed line includes an exaggerated correction for an excessively large centrifugal barrier, or low values of l_{\max} . One sees from the solid line helicity state counts that the low j_2 coincident states contribute most strongly to the vector correlation of the detected j_1 state, as the high helicity components ($|\lambda_1| > J + j_2$) are completely forbidden by angular momentum conservation. As the coincident j_2 increases, the allowed range of λ_1 broadens. The reasonable centrifugal barrier correction has no detectable effect on $p(\lambda_1)$ for coincident states $j_2 = 11$ or 22 , and can be seen to decrease the total state count by about 30% for $j_2 = 33$, preferentially depopulating low values of $|\lambda_1|$. Even the exaggerated centrifugal barrier has almost no effect on $p(\lambda_1)$ for $j_2 = 11$, while the preferential loss of low $|\lambda_1|$ states is evident at $j_2 = 22$. A strong reduction in the total probability of $j_1 = 35$ in coincidence with $j_2 = 33$ would result from the low l_{\max} implied by $b_{\max} = 1.0 \text{ \AA}$.

In Fig. 5 we represent the $p(\lambda_1)$ distributions by their second Legendre moments, $\langle P_2(\hat{\mathbf{v}}\cdot\hat{\mathbf{j}}_1) \rangle$, still as a function of coincident j_2 for fixed $J = 10$ and $j_1 = 35$. We see the strictly negative $\mathbf{v}\cdot\mathbf{j}$ correlation for the solid line helicity state count, with the strongest correlation at low j_2 . The effect of the centrifugal barrier is confined to $j_2 > 30$, near the energetic limit, where the net effect is to decrease the population, but in a way that drives the $\mathbf{v}\cdot\mathbf{j}$ correlation slightly positive, as noted by Klippenstein and Cline.⁶ These j_2 -dependent $\mathbf{v}\cdot\mathbf{j}$ correlations should be evident as a velocity-dependent $\mathbf{v}\cdot\mathbf{j}$

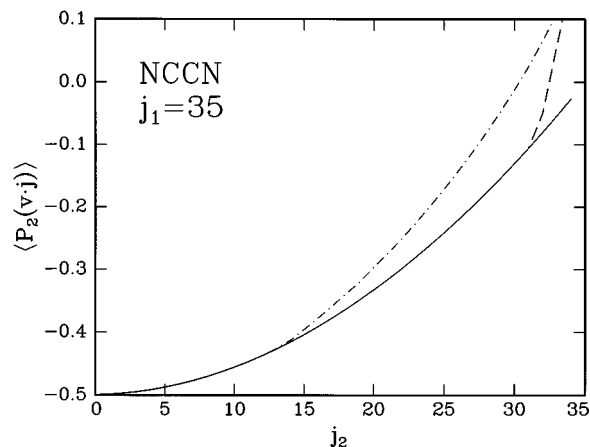


FIG. 5. Centrifugal barrier effects on the j_2 -dependent $v \cdot j_1$ correlations from a detected $j_1=35$ fragment and total $J=10$. The three lines are as described in Fig. 4.

correlations in the analysis of Doppler profiles, or analogous time-of-flight experiments, with speed distributions related to the coincident j_2 distributions. The coincident j_2 distributions are obtained by summing over the λ_1 state counts, and are shown in Fig. 6. These plots could as well have been prepared with the conventional PST for $b_{\max}=\infty$, 4.0 Å, and 1.0 Å, without reference to helicity states. The effect of the centrifugal barrier is seen to be a reduction in the highest coincident j_2 states. Finally, the global rotational distributions are shown in Fig. 7, obtained by summing over all coincident j_2 states as a function of j_1 for the same three centrifugal barrier cases at total $J=10$. The rotational distributions get colder as the effects of the centrifugal barrier become more severe, although at this level of averaging, it would be hard to distinguish an increase in the bond dissociation energy from a more restrictive l_{\max} .

We emphasize that although these corrections for the centrifugal barrier can be made, giving the exact PST vector

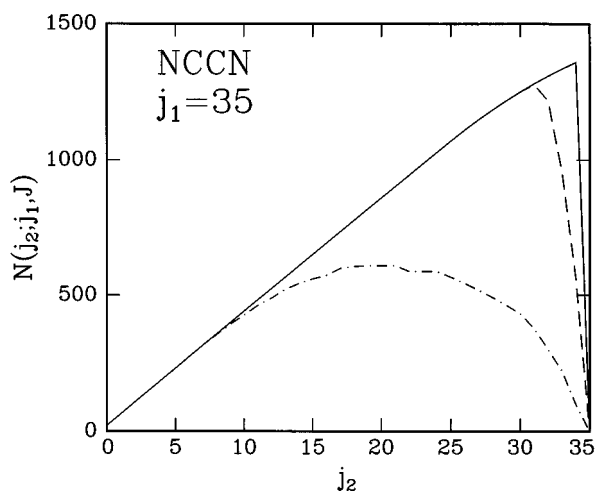


FIG. 6. Centrifugal barrier effects on the j_2 distribution formed in coincidence with $j_1=35$ from NCCN dissociation at fixed $J=10$. The three lines are as described in Fig. 4.

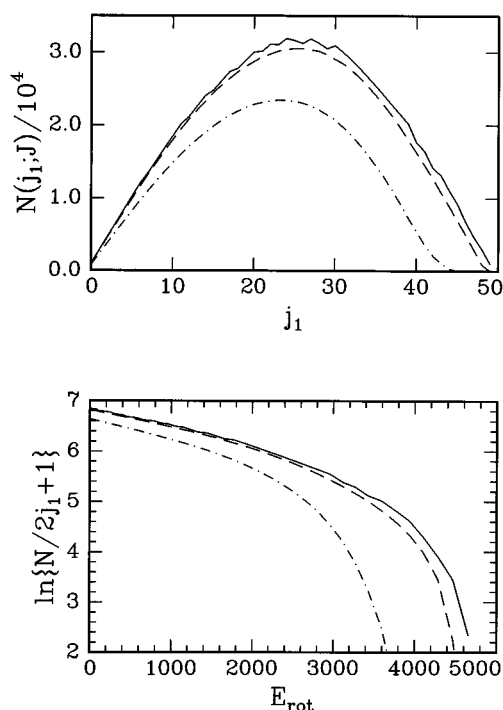


FIG. 7. Centrifugal barrier effects on the total $CN(v_1=0)$ rotational state distributions from NCCN dissociation assuming an available energy of 4700 cm^{-1} and total $J=10$. Only the coincident $CN v_2=0$ channel is shown. The three lines are as described in Fig. 4.

correlations, the far simpler helicity state count gives an intuitively useful and nearly quantitatively correct result in most cases. A simple and rapid integer calculation, comparing the total phase space state count, N , with the total helicity state count N' , will give a good idea ahead of time whether the correction is likely to be significant, and if a correction is warranted, whether the transformed PST or the corrected HSC will be less work.

III. SIMPLE EXAMPLES

As an example of the equivalence of the state counting, consider a single dissociation channel of a parent molecule with total angular momentum $J=2$ into a pair of diatomic fragments with rotational angular momenta $j_1=1$ and $j_2=1$. The conventional state count proceeds by combining j_1 and j_2 to give resultant j , which in this case can take on values of 0, 1, or 2 according to the triangle inequalities $\Delta(j, j_1, j_2)$. For each j , there will be a range of orbital angular momenta l that satisfy the triangle inequalities $\Delta(J, j, l)$. The nine possible jl states are enumerated in Table I. Each of these jl

TABLE I. PST state count.

jl states for $J=2, j_1=j_2=1$		
j	l	Count
0	2	1
1	1,2,3	3
2	0,1,2,3,4	5

TABLE II. Helicity state count.

$\lambda_1\lambda_2$ states for $J=2, j_1=j_2=1$		
λ_1	λ_2	Count
-1	-1,0,1	3
0	-1,0,1	3
1	-1,0,1	3

states has total $J=2$ and a corresponding additional $2J+1$ -fold degeneracy. To compute the $\mathbf{v}\cdot\mathbf{j}_1$ correlation of this channel with transformed PST is straightforward, each helicity state requiring a sum of contributions from each of the $9jl$ states. Summing over λ_2 to get $p(\lambda_1)$ would require evaluating $(9\times 9\times 2)$ $3-j$ symbols.

The same dissociation channel can be characterized by the helicity states of fragments 1 and 2, denoted by λ_1 and λ_2 . The angular momentum constraints are now embodied in the inequalities $|\lambda_1|\leq j_1$, $|\lambda_2|\leq j_2$, and $|\lambda_1-\lambda_2|\leq J$. In each case the inequality arises from a projection number bounded by the magnitude of the associated angular momentum. An enumeration of the $\lambda_1\lambda_2$ states consistent with the same J, j_1 , and j_2 is shown in Table II. Again, there are nine $\lambda_1\lambda_2$ states, each with total $J=2$ and five possible values of M . In this helicity representation, it is clear that all permitted values of λ_1 are equally likely in the state count, and the ratio 3:3:3 for $\lambda_1=-1:0:1$ corresponds to no $\mathbf{v}\cdot\mathbf{j}_1$ correlation, as can be verified by evaluating the sum in Eq. (7).

If the total angular momentum in this simple case is reduced to $J=1$, there are only seven allowed jl states which are shown in Table III. In this representation, it is hard to see that there is now a nonvanishing $\mathbf{v}\cdot\mathbf{j}_1$ correlation, although the count of $\lambda_1\lambda_2$ states in Table IV shows that the two states missing, compared to the uncorrelated case above for $J=2$, have total helicity $\lambda_1-\lambda_2=\pm 2$, which is not possible when the total J is 1. The relative probabilities of λ_1 are now 2:3:2 and the expectation value of $P_2(\hat{\mathbf{v}}\cdot\hat{\mathbf{j}}_1)$ is $-1/14$. Of course, the presence of rotational polarization is clear from a simple inspection of the λ_1 distribution. These illustrations show the identity of state counts in the conventional $|jl\rangle$ basis and in the helicity $|\lambda_1\lambda_2\rangle$ basis when the upper bound on l comes from angular momentum conservation and not energy conservation at the centrifugal barrier.

As a final example, suppose that for the kinetic energy of this product channel, the orbital angular momentum could not exceed 2, so that the single $l=3$ state needs to be removed from the phase space count. That is, $N'=7$, but $N=6$. This forbidden $|jl\rangle$ state, $|2,3\rangle$, can be expanded as a sum of $|\lambda_1\lambda_2\rangle$ states and its contribution removed from the

TABLE III. PST state count.

jl states for $J=1, j_1=j_2=1$		
j	l	Count
0	1	1
1	0,1,2	3
2	1,2,3	3

TABLE IV. Helicity state count.

$\lambda_1\lambda_2$ states for $J=1, j_1=j_2=1$		
λ_1	λ_2	Count
-1	-1,0	2
0	-1,0,1	3
1	0,1	2

$p'(\lambda_1)$ count. In this case, explicit evaluation of the $3-j$ symbols according to Eq. (6) shows that this jl state has contributions from all seven helicity components with the following amplitudes, a_i :

$$|jl\rangle = \sum_i a_i |\lambda_1\lambda_2\rangle_i, \quad (11)$$

$$|23\rangle = \frac{1}{\sqrt{10}} [|-1-1\rangle - |-10\rangle - |0-1\rangle + 2|00\rangle - |01\rangle + |1-1\rangle - |10\rangle].$$

The probability of measuring $\lambda_1=-1:0:1$ in the jl state $|23\rangle$ is related to the corresponding squared amplitudes, which occur in the ratio of 1/5:3/5:1/5. The normalized $p'(\lambda_1)$ was 2/7:3/7:2/7 from the previous example including all seven l states. The corrected, but unnormalized helicity distribution for fragment 1 is then $p(\lambda_1)=2-1/5:3-3/5:2-1/5$, which results in a weaker $\mathbf{v}\cdot\mathbf{j}_1$ correlation of $-1/20$ for the six jl states, compared to $-1/14$ when all l states are included. This is qualitatively expected, as the states with the largest l will generally impose a stronger constraint on the remaining angular momenta.

IV. APPLICATIONS

A. NCCN

1. Center-of-mass vector correlations

Considerable work has been reported on the ultraviolet spectroscopy, photophysics, and photochemistry of cyanogen, NCCN.¹⁴⁻¹⁷ The rotational state distributions measured by Eres *et al.*¹⁴ and others are well described by phase space theory. It has been generally accepted that the mechanism is internal conversion to and dissociation on a barrierless $^1\Sigma^+$ ground state. Recently, vector correlations have been observed by Wu and Hall for selected states of the CN photofragments from the 193 nm dissociation of NCCN.⁵ Although the $\mathbf{v}\cdot\mathbf{j}$ correlations were previously taken to indicate dynamical aspects to the dissociation, we now find they can be quantitatively modeled with the statistical calculations described here. Klippenstein and Cline have recently performed Monte Carlo evaluations of classical phase space integrals to estimate the statistical state-resolved, center-of-mass $\mathbf{v}\cdot\mathbf{j}$ correlations relevant to this system.⁶ We have subsequently calculated the equivalent quantities quantum mechanically using the theory outlined above. For our calculations, $p'(\lambda_1)$ was computed for selected states j_1 , with $v_1=0$ and 1, averaged over coincident j_2 , treating $v_2=0$ and 1 separately, for various values of J . The helicity state counts

TABLE V. Calculated vector correlations $\beta_0^0(22)$ for $v=0$, j_{CN} selected CN fragments from NCCN: comparison of the uncorrected helicity state count (HSC) with the corrected helicity state count (CHSC).

J_{NCCN}	Coincident CN $v=0$							
	$j_{\text{CN}}=17$		$j_{\text{CN}}=30$		$j_{\text{CN}}=35$		$j_{\text{CN}}=40$	
	HSC	CHSC	HSC	CHSC	HSC	CHSC	HSC	CHSC
0	-0.057 ^a	-0.058	-0.160	-0.159	-0.257	-0.259	-0.372	-0.377
10	-0.046	-0.047	-0.146	-0.150	-0.232	-0.232	-0.338	-0.340
20	-0.029	-0.029	-0.119	-0.119	-0.173	-0.176	-0.248	-0.249
30	-0.021	-0.022	-0.077	-0.075	-0.110	-0.106	-0.155	-0.148
40	-0.016	-0.016	-0.042	-0.039	-0.056	-0.050	-0.075	-0.063
60	-0.001	0.002	-0.005	0.002	-0.006	0.007	-0.007	0.020
	Coincident CN $v=1$							
0	-0.090	-0.090	-0.370	-0.379	-0.472	-0.481
10	-0.074	-0.073	-0.311	-0.314	-0.428	-0.432
20	-0.046	-0.046	-0.184	-0.182	-0.300	-0.284
30	-0.026	-0.025	-0.076	-0.063	-0.119	-0.068
40	-0.008	-0.005	-0.020	-0.003	-0.022	-0.043
60	0.000	0.003	0.000	0.023	0.000	0.057	0.000	-0.057
Thermal ^c	-0.021		-0.061		-0.075		...	-0.094
$\Lambda_{\text{NCCN}}=1$	-0.062		-0.154		-0.195		...	-0.236
Expt. ^d	-0.08±0.04		-0.15±0.06		-0.21±0.04		...	-0.23±0.04

^aCenter-of-mass frame.^b... indicates energetically inaccessible states.^cCorrected for the center-of-mass to laboratory frame transformation.^dReference 5.

(HSC) were made assuming an available energy of 4700 cm^{-1} to compare to the classical calculations of Klippenstein and Cline. The results of both the uncorrected (HSC) and corrected calculations (CHSC) are presented in Tables V and VI. For all state combinations examined, the agreement between the classical⁶ and corrected quantum $\mathbf{v}\cdot\mathbf{j}$ correlations is exact, within small Monte Carlo sampling errors. The uncorrected $\mathbf{v}\cdot\mathbf{j}$ correlations, $\beta_0^0(22)$, calculated by ignoring the centrifugal barrier, agree very well with the corrected state count, particularly at low J , as one might expect. Both the trends and the magnitudes of the $\mathbf{v}\cdot\mathbf{j}$ correlations with total J and with the fragment j are reproduced correctly, except for the small positive correlation predicted by the CHSC calcu-

lations at high total J and high fragment j , which is absent in the uncorrected calculations. This difference occurs for those channels where the centrifugal barrier should be most significant. We should mention that for small molecules with modest energies like this, the present state counting approach is much faster than the Monte Carlo phase space algorithm of Klippenstein and Cline.⁶ To compute the HSC results shown in Tables V and VI required only a few seconds on a 80486-based personal computer, although the CHSC results shown required about an hour of additional computer time.

2. Thermal averaging and laboratory frame transformation

To compare to thermal experiments the degradation of the center-of-mass $\mathbf{v}\cdot\mathbf{j}$ correlations due to the distribution of

TABLE VI. Calculated vector correlations $\beta_0^0(22)$ for $v=1$, j_{CN} selected CN fragments from NCCN: comparison of the uncorrected helicity state count (HSC) with the corrected helicity state count (CHSC).

J_{NCCN}	Coincident CN $v=0$							
	$j_{\text{CN}}=6$		$j_{\text{CN}}=11$		$j_{\text{CN}}=16$		$j_{\text{CN}}=21$	
	HSC	CHSC	HSC	CHSC	HSC	CHSC	HSC	CHSC
0	-0.024 ^a	-0.025	-0.047	-0.048	-0.080	-0.081	-0.133	-0.136
10	-0.008	-0.008	-0.029	-0.030	-0.064	-0.065	-0.118	-0.119
20	-0.005	-0.005	-0.017	-0.017	-0.041	-0.040	-0.077	-0.076
30	-0.004	-0.004	-0.013	-0.012	-0.024	-0.023	-0.037	-0.035
40	-0.001	-0.001	-0.004	-0.002	-0.007	-0.005	-0.011	-0.007
60	0.000	0.000	0.000	0.001	0.000	0.003	0.000	0.005
Thermal ^b		-0.003		-0.009		-0.017		-0.030
$\Lambda_{\text{NCCN}}=1$		-0.020		-0.041		-0.067		-0.111
Expt. ^c		-0.01±0.04		-0.02±0.06		-0.14±0.06		-0.08±0.06

^aCenter-of-mass frame.^bCorrected for the center-of-mass to laboratory frame transformation.^cReference 5.

parent velocities must be taken into account prior to averaging over coincident j_2 states. The procedure is similar to the treatment of degraded spatial anisotropy in photodissociation and in photoinitiated bimolecular reactions.¹⁸ The azimuthally averaged addition (AAA) theorem¹⁹ permits evaluation of the effective, laboratory $\mathbf{v}\cdot\mathbf{j}$ correlation in terms of the center-of-mass ($\mathbf{u}\cdot\mathbf{j}$) correlation and a laboratory to center-of-mass factor, provided \mathbf{j} is azimuthally symmetric about the center-of-mass velocity, \mathbf{u}

$$\langle P_2(\hat{\mathbf{v}}\cdot\hat{\mathbf{j}}) \rangle = \langle P_2(\hat{\mathbf{v}}\cdot\hat{\mathbf{u}}) \rangle \langle P_2(\hat{\mathbf{u}}\cdot\hat{\mathbf{j}}) \rangle. \quad (12)$$

The Boltzmann average over parent velocities can be performed analytically,²⁰ giving

$$\beta_0^0(22)_{\text{lab}}(v, j_2) = \frac{\beta_0^0(22)_{j_2} I_{5/2}(vu/\sigma^2)}{I_{1/2}(vu/\sigma^2)}, \quad (13)$$

$\mathbf{v}\cdot\mathbf{j}$ correlations as a function of laboratory velocity \mathbf{v} for each j_2 state with its center-of-mass velocity u , where $I_{5/2}$ and $I_{1/2}$ are modified spherical Bessel functions, $\sigma^2 = (k_B T/m)$, and $\beta_0^0(22)_{j_2}$ is the center-of-mass $\mathbf{u}\cdot\mathbf{j}$ vector correlation for a specific j_2 state. The corresponding laboratory velocity distribution for each j_2 is given by,

$$f(\mathbf{v}, j_2) = \frac{\exp[-(v^2 + u^2)/2\sigma^2] I_{1/2}(vu/\sigma^2)}{4\pi\sigma^2 \sqrt{vu}}. \quad (14)$$

The laboratory frame velocity distribution is then given by

$$f(\mathbf{v}) = \sum_{j_2} P(j_2) \times f(\mathbf{v}, j_2) \quad (15)$$

with $P(j_2)$ the normalized distribution of j_2 for fixed j_1 and J , and the velocity-dependent $\mathbf{v}\cdot\mathbf{j}$ correlation in the laboratory frame is

$$\beta_0^0(22)_{\text{lab}}(v) = \frac{\sum_{j_2} \beta_0^0(22)_{\text{lab}}(v, u_{j_2}) \times P(j_2) \times f(\mathbf{v}, u_{j_2})}{\sum_{j_2} P(j_2) \times f(\mathbf{v}, u_{j_2})}. \quad (16)$$

The laboratory frame, velocity-averaged $\mathbf{v}\cdot\mathbf{j}$ correlation for each parent J is then

$$\beta_0^0(22)_{\text{lab}} = 4\pi \int_0^\infty \beta_0^0(22)_{\text{lab}}(v) \times f(v) v^2 dv. \quad (17)$$

The rows of Tables V and VI labeled ' $\Lambda_{\text{NCCN}}=1$ ' are obtained in this way for $J=1$. A Boltzmann average over parent J finally gives the thermal $\mathbf{v}\cdot\mathbf{j}$ correlations for each detected j_1 state, labeled "Thermal" in the same tables, where coincident $v_2=0$ and $v_2=1$ states were combined with phase space theory weights.

3. Comparison to experiment

The general trend of an increasingly strong tendency for \mathbf{j} to be perpendicular to \mathbf{v} at higher rotational levels is common to the theory and the experimental results of Wu and Hall.⁵ A key difference is that the observed vector correlation is more than twice as large as the thermally averaged, statistical expectation. It seems very likely that this is a consequence of an additional constraint on the dissociation of the

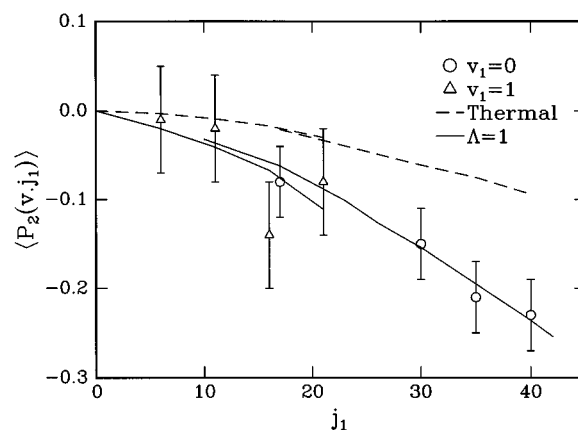


FIG. 8. Comparison of experimental⁵ and calculated $\mathbf{v}\cdot\mathbf{j}$ correlations for CN fragments from the 193 nm dissociation of NCCN. Dashed lines are fully averaged thermal calculations and solid lines are for the restricted helicity model. Selected rotational states j_1 of the detected states $v_1=0$ and 1 are shown; the calculated lines for $v_1=1$ extend from $j_1=0$ to 21.

linear molecule, NCCN. In computing the state distribution, the total helicity of the two fragments is allowed to range between $+J$ and $-J$ of the parent molecule. In the axial recoil limit, where the radial velocity of the fragments far exceeds their tangential velocity, the combined helicity of the two fragments is closely identified with the projection of total J around the axis of the linear molecule, which necessarily vanishes. The spectroscopically populated levels of the predissociating NCCN $A^1\Sigma_u^-$ and $B^1\Delta_u^-$ states reached by Herzberg–Teller interaction are characterized by a single unit of vibrational angular momentum, $K=1$. If this body-fixed projection number is not mixed in the internal conversion to the ground state or in the separation of CN products, we should expect the total helicity to remain small, even in a thermal sample of NCCN with large values of total J . For this special case of linear molecule dissociation, the angular momentum conservation constraint in the helicity basis is more severe than shown in Eq. (9), as the value of $|\lambda_1 - \lambda_2|$ is bounded by K , rather than J

$$N'_{\text{linear}}(E, J) = \sum_{v_1, j_1, \lambda_1, v_2, j_2, \lambda_2, M} \Theta[E - E_1(v_1, j_1) - E_2(v_2, j_2)] \times \Theta(K - |\lambda_1 - \lambda_2|). \quad (18)$$

Restricting the K states (or the total helicity, Λ) to 0 and 1, even in a room temperature sample including high J states, produces vector correlations identical to those obtained with total $J=1$. The $\Lambda_{\text{NCCN}}=1$ rows of Tables V and VI, which include the center-of-mass to laboratory correction, are in quantitative agreement with the experimentally determined $\mathbf{v}\cdot\mathbf{j}$ correlations, lending support to this notion of K restriction in a linear molecule leading to enhanced $\mathbf{v}\cdot\mathbf{j}$ correlation. Figure 8 shows the bottom three rows of Tables V and VI: the laboratory frame, thermally averaged $\mathbf{v}\cdot\mathbf{j}$ correlations as a function of the detected j_{CN} states in vibrational levels 0 and 1, the linear molecule limit of the calculated $\mathbf{v}\cdot\mathbf{j}$ correlations, where the total helicity is less than or equal to 1, along with the experimental measurements.

TABLE VII. Calculated vector correlations $\beta_0^0(22)$ for $v=0$, j_{CN} selected CN fragments from NCNO, averaged over all possible coincident $v=0$, j_{NO} .

J_{NCNO}	$j_{\text{CN}}=5$	$j_{\text{CN}}=10$	$j_{\text{CN}}=15$	$j_{\text{CN}}=25$
		$E_{\text{avail}}=411 \text{ cm}^{-1}$		
Jet	-0.034	-0.175	... ^a	...
Bulb ^b	-0.001	-0.004
		$E_{\text{avail}}=939 \text{ cm}^{-1}$		
Jet	-0.019	-0.074	-0.192	...
Bulb	-0.002	-0.007	-0.014	...
		$E_{\text{avail}}=1670 \text{ cm}^{-1}$		
Jet	-0.014	-0.045	-0.097	-0.382
Bulb	-0.002	-0.009	-0.018	-0.034

^a... indicates energetically inaccessible states.

^bThermal average over parent rotational distributions. The values of $\beta_0^0(22)$ are given in the laboratory frame.

We now provide a cautionary note regarding the ability of the experimental $\mathbf{v}\cdot\mathbf{j}$ correlations to address discrepancies in the value of $D_0^0(\text{NCCN})$. The bond dissociation energy advocated by Huang *et al.*²¹ and others¹⁴⁻¹⁶ would correspond to 4700 cm^{-1} of excess energy following photodissociation at 193 nm. Although we have found excellent agreement in the $\mathbf{v}\cdot\mathbf{j}$ correlations using an available energy of 4700 cm^{-1} in the calculations shown here, the agreement is not particularly sensitive to this choice of energy. The center-of-mass $\mathbf{v}\cdot\mathbf{j}$ correlations depend on the available energy, increasing as the available energy decreases. The laboratory $\mathbf{v}\cdot\mathbf{j}$ correlations are not as sensitive since decreasing the available energy also reduces the center-of-mass velocities, resulting in a more severe thermal degradation of the $\mathbf{v}\cdot\mathbf{j}$ correlation. Wu and Hall⁵ found that the wings of the Doppler profiles, a direct measure of the fastest coincident fragments, were consistent with an available energy closer to 5300 cm^{-1} .²² Recalculating the $\Lambda_{\text{NCCN}}=1$ rows of Tables V and VI using an available energy of 5300 cm^{-1} also gives vector correlations within the experimental uncertainties.

Further questions remain about the true available energy, the possible role of an exit barrier in the dissociation, kinetic shifts in the threshold for detecting CN fragments, and the relationship between the available energy, the state distributions, and the vector correlations. New experimental work is in progress.^{23,24} We are optimistic about resolving the speed-dependent $\mathbf{v}\cdot\mathbf{j}$ correlation in our next generation of Doppler spectroscopy experiments, which is related to the coincident j_2 -dependent helicity distribution. Much of the apparent deviation from statistical behavior in the photodissociation of NCCN may well turn out to be related to changes in the form of the statistical theory to treat the special case of angular momentum conservation in linear polyatomic molecules.

B. NCNO

The predissociation of NCNO has been thoroughly characterized through numerous experiments by Wittig and co-workers.^{3,25,26} As a result NCNO has become a benchmark system for testing statistical theories of unimolecular dissociation. Initial experiments focused on global product rotational and vibrational state distributions. At excess ener-

gies below the threshold for vibrational excitation in the products ($E < 1860 \text{ cm}^{-1}$) the state distributions were remarkably well reproduced using PST. At higher energies, with the possibility of fragment vibrational excitation, experimental distributions deviated from PST, leading to the suggestion of a modified theory of separate statistical ensembles (SSE).¹¹

Experiments by Qian *et al.*²⁶ measured correlated scalar distributions in the dissociation using Doppler spectroscopy of CN $B^2\Sigma^+ \leftarrow X^2\Sigma^+$ lines at excess energies between 411 and 2348 cm^{-1} . The experiments provided a more stringent test for both PST and the SSE model. No deviations from the barrierless dissociation models were detected, in contrast to statistical adiabatic channel model²⁷ prediction of exit barriers arising from the adiabatic evolution of parent vibrations into product rotations. No $\mathbf{v}\cdot\mathbf{j}$ vector correlations were reported by Qian *et al.*, although an excess population of the A' lambda doublet level of NO was detected for the highest J states.²⁶ We have calculated the j_{NO} averaged $\beta_0^0(22)$ values for selected j_{CN} rotational states at three excess energies (411 , 939 , and 1670 cm^{-1}), each below the threshold for

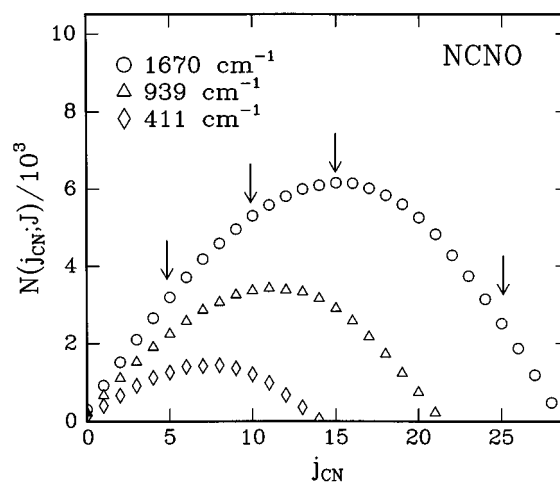


FIG. 9. CN($v=0$) rotational distributions from NCNO, obtained using PST for three values of the available energy. The arrows indicate the j_1 states for which the $\mathbf{v}\cdot\mathbf{j}_1$ correlation has been calculated and shown in Table VII.

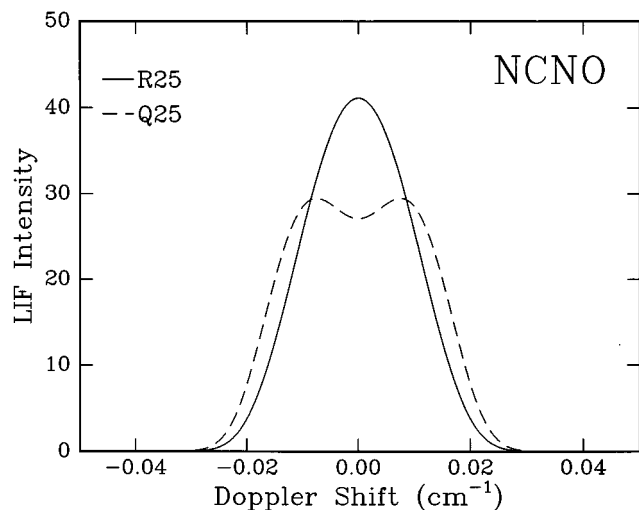


FIG. 10. Simulated R branch (solid line) and Q branch (dashed line) Doppler profiles predicted for detected CN ($j=25$, $v=0$) arising from the jet-cooled photodissociation of NCNO at 1670 cm^{-1} available energy.

formation of NO $v=1$. For reference, Fig. 9 shows the j_{CN} rotational state distributions at these available energies as predicted by PST, with arrows indicating the CN states for which the $\mathbf{v}\cdot\mathbf{j}_{\text{CN}}$ correlation was calculated. A value of $b_{\text{max}}=4.0\text{ \AA}$ for the centrifugal barrier was taken from the work of Klippenstein.²⁸ Table VII contains the results of the calculations for parent rotation states characteristic of jet-cooled sample ($J=5$) and a fully averaged room temperature sample. The results are qualitatively similar to those shown in Table V and VI for NCCN dissociation. The $\mathbf{v}\cdot\mathbf{j}_{\text{CN}}$ correlation is weak in the thermal sample, but several of the states detected by Qian *et al.*²⁶ from jet-cooled NCNO should have possessed strong vector correlations. Modeling the Doppler line shapes expected for statistically populated CN states, we find that dramatic differences in Q and R -branch lines of CN should be detectable in a higher resolution experiment; an example with 0.01 cm^{-1} resolution at 700 nm is shown in Fig. 10. The choice of the $B-X$ transition, with no Q branch, combined with limited spectral resolution and slow fragments made these effects undetectable under the experimental conditions used by Qian *et al.* Currently work is underway in our group to measure Doppler profiles using $A-X$ LIF CN detection in a jet to test these predicted $\mathbf{v}\cdot\mathbf{j}_{\text{CN}}$ correlations for selected j_{CN} states.

C. CH₂CO

As a final example we consider the ground state dissociation of ketene, CH₂CO, another classic barrierless dissociation.^{4,29,30} State distributions for both CO and CH₂ fragments have been reported at a variety of wavelengths near the threshold for singlet CH₂, and photofragment excitation spectra have provided a remarkably detailed view of the dissociation process to compare with unimolecular reaction theory. Coincident CO product state distributions have been measured for low J singlet CH₂ fragments following 308 nm dissociation by Doppler spectroscopy in this

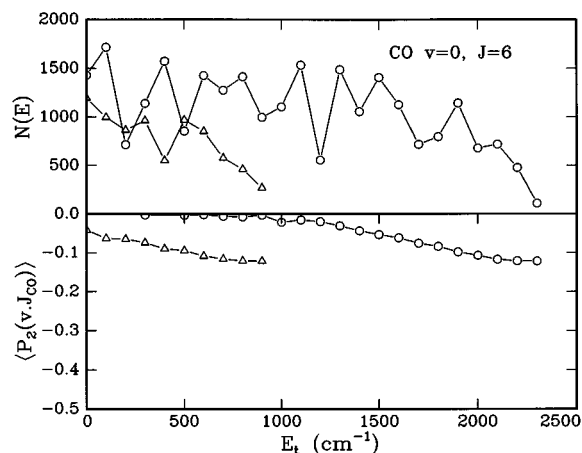


FIG. 11. Phase space theory calculation of state-resolved CO translational energy distributions, and CO $\mathbf{v}\cdot\mathbf{j}$ vector correlation as a function of translational energy for ketene photolysis at 308 nm . The contribution of CH₂ (000) states is shown with circles, that of CH₂ (010) is shown with triangles. Results for $j_{\text{CO}}=6$ are shown.

laboratory.³¹ The coincident CO rotational distributions were found to agree with PST calculations, but showed an excess population of CO $v=1$ compared to PST calculations. No sign of velocity anisotropy or $\mathbf{v}\cdot\mathbf{j}$ correlations was observed for the low J CH₂ states observed. Analogous experiments sensitive to the CH₂ coincident energies for spectroscopically selected CO states have recently been performed using a metastable time-of-flight technique in Wodtke's laboratory.³² The TOF signals show vibrationally resolved peaks, assigned to CO in coincidence with singlet CH₂ with one or no quanta of bending energy, as well as a small amount of faster CO produced in coincidence with triplet CH₂. The TOF signals show strong probe laser polarization effects,³³ which should be understandable in terms of coincident-state-dependent CO $\mathbf{v}\cdot\mathbf{j}$ correlations with appropriate center-of-mass to laboratory frame transformations.

We have performed helicity state counts for the ketene photodissociation conditions relevant to the metastable CO TOF experiments of Drabbels *et al.*³² The coincident state counts of singlet CH₂ for selected CO fragment states were computed at an available energy of 2351 cm^{-1} and a parent $J=5$, typical of jet-cooled ketene. The CH₂ state counts, in 100 cm^{-1} translational energy bins, are shown in the top panels of Figs. 11 and 12 for $j_{\text{CO}}=6$ and 17. Separate counts are shown for CH₂ with no vibrational excitation (○) and for CH₂ with a single quantum of bending excitation (△). A centrifugal barrier at b_{max} between 3 and 5 \AA has no effect on these distributions whatever, and the helicity state count is equivalent to the full phase space theory. The $\mathbf{v}\cdot\mathbf{j}$ correlations are plotted as a function of kinetic energy in the lower panels of Figs. 11 and 12, with separate plots for the CH₂ (000) state and the (010) state, as before. The fastest CO in $j=17$ corresponds to low j states of the coincident CH₂ and these CO states must have a strong $\mathbf{v}\perp\mathbf{j}$ tendency. The calculated coincident CH₂ internal energy distributions are evidently hotter than the experimental distributions observed by Drabbels *et al.*,³² as the calculated global CH₂ state distributions are

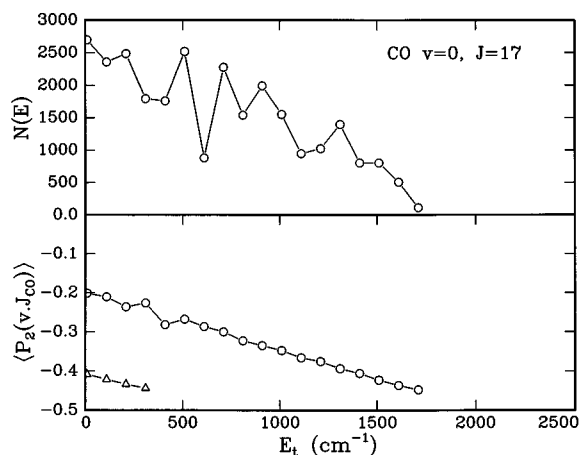


FIG. 12. Same as Fig. 11, but for $j_{CO}=17$.

similarly hotter than those measured in the Moore group.²⁹ The peculiar observation that the CO state distribution is reasonably well described by phase space theory, while the CH₂ is significantly colder is unrelated to centrifugal barriers or angular momentum constraints, since the missing CH₂ states have lower angular momentum than the typical CO states that are observed. We consider this question as a major unresolved challenge in the understanding of ketene dissociation,³⁴ and expect that a careful look at the correlated fragment properties may provide useful clues.

As an aside, the absence of detectable $\mathbf{v} \cdot \mathbf{j}$ correlations in the CH₂ Doppler spectroscopy³¹ is fully consistent with the HSC calculations for ketene, which give -0.003 for the thermally averaged $\beta_0^0(22)$ for a $J=4$ CH₂ state. One never expects to find significant $\mathbf{v} \cdot \mathbf{j}$ correlations in a fragment whose j is less than the typical coincident j or the total J , a qualitative observation also noted by Klippenstein and Cline.⁶

V. CONCLUSION

In conclusion, a quantum formulation of phase space theory using the helicity basis has been presented which provides a computationally rapid and intuitively simple means to obtain a statistical prediction of $\mathbf{v} \cdot \mathbf{j}$ correlations in molecular photodissociation. To include the effects of centrifugal barriers adds some complexity to the theory, but the corrections can be made exactly if necessary, and a simple integer calculation gives an estimate of the importance of the correction. We have compared the statistical predictions of $\mathbf{v} \cdot \mathbf{j}$ correlations with experiment in the case of NCCN, and predicted the magnitude of $\mathbf{v} \cdot \mathbf{j}$ correlations that have not yet been observed in NCNO, and observed, but not yet analyzed in the case of CH₂CO, three small molecules whose photodissociations are reasonably well described by phase space theory.

ACKNOWLEDGMENTS

G.E.H. acknowledges Professor Stephen Klippenstein for extensive discussions on the topic of statistical theories and vector correlations, and for providing a prepublication

copy of Ref. 6, and thanks Professor A. M. Wodtke for sharing prepublication information on his ketene experiments. This work was performed at Brookhaven National Laboratory under Contract No. DE-AC02-76CH00016 with the U.S. Department of Energy and supported by its Division of Chemical Sciences.

- ¹P. Pechukas and J. C. Light, *J. Chem. Phys.* **42**, 3281 (1965); P. Pechukas, J. C. Light, and C. Rankin, *ibid.* **44**, 794 (1966); J. C. Light, *Discuss. Faraday Soc.* **44**, 14 (1967); C. E. Klots, *J. Phys. Chem.* **75**, 1526 (1971).
- ²J. C. Light, *Atom-Molecule Collision Theory: A Guide for the Experimentalist*, edited by R. B. Bernstein (Plenum, New York, 1979), and references therein.
- ³H. Reisler and C. Wittig, *Annu. Rev. Phys. Chem.* **37**, 307 (1986).
- ⁴W. H. Green, Jr., C. B. Moore, and W. F. Polik, *Annu. Rev. Phys. Chem.* **43**, 591 (1992).
- ⁵M. Wu and G. E. Hall, *J. Photochem. Photobiol. A: Chem.* **80**, 45 (1994).
- ⁶S. J. Klippenstein and J. Cline, *J. Chem. Phys.* **103**, 5451 (1995).
- ⁷G. E. Hall, SPIE Proceedings Series No. 2548, *Laser Techniques for State-Selected and State-to-State Chemistry*, San Diego, CA, July 1995.
- ⁸R. N. Dixon, *J. Chem. Phys.* **85**, 1866 (1986).
- ⁹M. Jacob and G. C. Wick, *Ann. Phys.* **7**, 404 (1959).
- ¹⁰P. J. Dagdigian, H. W. Cruse, A. Shultz, and R. N. Zare, *J. Chem. Phys.* **61**, 4450 (1974).
- ¹¹C. Wittig, I. Nadler, H. Reisler, M. Noble, H. J. Catanzarite, and G. Radhakrishnan, *J. Chem. Phys.* **83**, 5581 (1985).
- ¹²R. N. Zare, *Angular Momentum* (Wiley, New York, 1988).
- ¹³K. Schulten and R. G. Gordon, *J. Math. Phys.* **16**, 1971 (1975).
- ¹⁴D. Eres, M. Gurnick, and J. D. McDonald, *J. Chem. Phys.* **81**, 5552 (1984).
- ¹⁵J. B. Halpern and W. M. Jackson, *J. Phys. Chem.* **86**, 973 (1982); H. Lin, E. A. Johnson, and W. M. Jackson, *Chem. Phys. Lett.* **152**, 477 (1988).
- ¹⁶E. A. J. Wannemacher, H. Lin, and W. M. Jackson, *J. Phys. Chem.* **94**, 6608 (1990).
- ¹⁷Y. Huang, Ph.D. dissertation, Howard University, 1993.
- ¹⁸E. P. Gilbert, G. Maitland, A. Watson, and K. G. McKendrick, *J. Chem. Soc. Faraday Trans.* **89**, 1527 (1993); F. Green, G. Hancock, A. J. Orr-Ewing, M. Brouard, S. P. Duxon, P. A. Enriquez, R. Sayos, and J. P. Simons, *Chem. Phys. Lett.* **182**, 568 (1991).
- ¹⁹J. D. Barnwell, J. G. Loesser, and D. R. Hershbach, *J. Phys. Chem.* **87**, 2781 (1983).
- ²⁰C. D. Jonah, R. N. Zare, and C. Ottinger, *J. Chem. Phys.* **56**, 263 (1972).
- ²¹Y. Huang, S. A. Barts, and J. B. Halpern, *J. Phys. Chem.* **96**, 425 (1992).
- ²²Recent high level *ab initio* calculations estimate the NCCN bond dissociation energy to be 132.8 ± 2 kcal mol⁻¹ which would correspond to an available energy at 193.3 nm of 5253 cm⁻¹; J. S. Francisco and S. L. Richardson, *J. Chem. Phys.* **102**, 1100 (1995).
- ²³S. W. North, X. S. Zheng, R. Fei, and G. E. Hall, *J. Chem. Phys.* (to be published).
- ²⁴S. W. North and G. E. Hall (unpublished results).
- ²⁵M. Noble, I. Nadler, H. Reisler, and C. Wittig, *J. Chem. Phys.* **81**, 4333 (1984); I. Nadler, M. Noble, H. Reisler, and C. Wittig, *ibid.* **82**, 2608 (1985); C. X. W. Qian, M. Noble, I. Nadler, H. Reisler, and C. Wittig, *ibid.* **83**, 5573 (1985).
- ²⁶C. X. W. Qian, A. Ogai, H. Reisler, and C. Wittig, *J. Chem. Phys.* **90**, 209 (1989).
- ²⁷M. Quack and J. Troe, *Ber. Bunsenges. Physik Chem.* **78**, 240 (1974).
- ²⁸S. J. Klippenstein, *J. Chem. Phys.* **101**, 1996 (1994).
- ²⁹D. J. Nesbitt, H. Petek, M. F. Foltz, S. V. Filseth, D. J. Bamford, and C. B. Moore, *J. Chem. Phys.* **83**, 223 (1985); I.-C. Chen, W. H. Green, Jr., and C. B. Moore, *ibid.* **89**, 314 (1988); I. Garcia-Moreno, E. R. Lovejoy, and C. B. Moore, *ibid.* **100**, 8890 (1994).
- ³⁰S. J. Klippenstein and R. A. Marcus, *J. Chem. Phys.* **91**, 2280 (1989); J. Yu and S. J. Klippenstein, *J. Phys. Chem.* **101**, 9882 (1991).
- ³¹B.-C. Chang, M. Wu, G. E. Hall, and T. J. Sears, *J. Chem. Phys.* **101**, 9236 (1994).
- ³²M. Drabbles, C. G. Morgan, D. S. McGuire, and A. M. Wodtke, *J. Chem. Phys.* **102**, 611 (1995).
- ³³M. Drabbles, C. G. Morgan, and A. M. Wodtke, *Conference on the Dynamics of Molecular Collisions*, Asilomar, CA, July 1995.
- ³⁴S. C. Smith, *Chem. Phys. Lett.* **243**, 359 (1995).